NIH Public Access
Author Manuscript
Science. Author manuscript; available in PMC 2014 September 09.

Published in final edited form as:
Science. 2014 January 17; 343(6168): 309–313. doi:10.1126/science.1248627.

Direct in Vivo RNAi Screen Unveils Myosin IIa as a Tumor Suppressor of Squamous Cell Carcinomas

Daniel Schramek[1], **Ataman Sendoel**[1], **Jeremy P. Segal**[1,*], **Slobodan Beronja**[1], **Evan Heller**[1], **Daniel Oristian**[1], **Boris Reva**[2], and **Elaine Fuchs**[1,†]

[1]Howard Hughes Medical Institute, Laboratory of Mammalian Cell Biology and Development, The Rockefeller University, New York, NY 10065, USA

[2]Department of Genetics and Genomic Science, Institute for Genomics and Multiscale Biology, Icahn School of Medicine at Mount Sinai, 1428 Madison Avenue, New York, NY 10029, USA

Abstract

Mining modern genomics for cancer therapies is predicated on weeding out “bystander” alterations (nonconsequential mutations) and identifying “driver” mutations responsible for tumorigenesis and/or metastasis. We used a direct in vivo RNA interference (RNAi) strategy to screen for genes that upon repression predispose mice to squamous cell carcinomas (SCCs). Seven of our top hits—including *Myh9*, which encodes nonmuscle myosin IIa—have not been linked to tumor development, yet tissue-specific *Myh9* RNAi and *Myh9* knockout trigger invasive SCC formation on tumor-susceptible backgrounds. In human and mouse keratinocytes, myosin IIa's function is manifested not only in conventional actin-related processes but also in regulating posttranscriptional p53 stabilization. Myosin IIa is diminished in human SCCs with poor survival, which suggests that in vivo RNAi technology might be useful for identifying potent but low-penetrance tumor suppressors.

Squamous cell carcinomas of the head and neck (HNSCCs) are the sixth most common human cancer worldwide, with frequent, often aggressive recurrence and poor prognosis (1). Established genetic and epigenetic alterations include *EGFR* amplifications; *Trp53, H-RAS, NOTCH*, PI3K/Akt, and *BRCA1* mutations; and transforming growth factor–β (TGF-β) pathway repression (1). Recent whole-exome sequencing efforts have revealed hundreds of additional “lower-penetrance” HNSCC mutations with unknown functional importance (2, 3).

To functionally test putative “driver mutations” that confer a selective advantage and contribute to tumor progression, researchers have used RNA interference (RNAi) followed by allografting of transduced cultured cancer cells. However, orthotopic transplantations necessitate immunocompromised animals and generate wound responses, which can confound physiological relevance. We have circumvented these difficulties with

Copyright 2014 by the American Association for the Advancement of Science; all rights reserved

†Corresponding author. fuchslb@rockefeller.edu.
*Present address: Department of Pathology, University of Chicago, Chicago, IL 60637, USA.

Supplementary Materials www.sciencemag.org/content/343/6168/309/suppl/DC1

NIH-PA Author Manuscript
NIH-PA Author Manuscript
NIH-PA Author Manuscript

NIH-PA Author Manuscript

NIH-PA Author Manuscript

NIH-PA Author Manuscript

noninvasive, ultrasound-guided in utero lentiviral-mediated RNAi delivery, selectively transducing single-layered surface ectoderm of living mouse embryos at embryonic day (E) 9.5 (4).

We first showed that mice transduced with *Brca1* short hairpin RNAs (shRNAs) that silence *BRCA1* expression recapitulate the *Brca1*-knockout phenotype and develop spontaneous skin and oral SCCs with long latency (5) (fig. S1). We accelerated tumor growth by testing hairpins in epithelial-specific, *TGF*β*-Receptor-II* conditional knockout (cKO) mice (*K14-Cre*;*T*β*RII*$^{floxed/floxed}$), which lose TGF-β signaling in skin, oral, and anogenital epithelia and display enhanced SCC susceptibility (6, 7). On this *T*β*RII*-cKO background, *Brca1* knockdown generated SCCs with increased frequency and a factor of 4 decrease in latency (fig. S1). Having validated our sensitized approach, we devised a pooled shRNA format to carry out an in vivo screen for additional putative suppressors of SCCs (Fig. 1A).

We selected 1762 shRNA lentiviruses targeting 347 mouse genes that either (i) had human orthologs carrying recurring HNSCC somatic mutations (2, 3) or (ii) were deregulated by a factor of ≥2 in tumor-initiating stem cells purified from SCCs initiated by oncogenic *HRas* (8) (table S1). We also included positive (*Brca1* shRNA) and negative (scrambled nontargeting shRNA) controls. After infecting E9.5 epidermis, we isolated E12.5 genomic DNA and verified by Illumina sequencing that shRNA representations correlated nicely with their individual abundance within our initial test pool (fig. S2).

To ensure a coverage of >500 individual clones per shRNA, we infected 74 genotypically matched *T*β*RII*-cKO or *T*β*RII*$^{fl/fl}$ control embryos with our lentivirus pool and monitored pups into adulthood. As expected (6), ~5% of the *T*β*RII*-cKO mice developed anogenital SCCs. Scrambled shRNA expression did not affect these statistics, nor did transduction with a “control pool” of 1000 random shRNAs. In contrast, all 28 library-transduced *T*β*RII*-cKO mice developed lesions within skin, the oral cavity, and/or mucocutaneous junctions at eyelids (Fig. 1B). These findings underscore the efficacy of our approach and document the enrichment of our test shRNA library for SCC tumor suppressors.

Most lesions displayed histopathological features of SCCs with varying degrees of differentiation and local invasion; a few were squamous papillomas or epidermal hyperplastic lesions (figs. S3 to S5). Sequencing revealed that most lesions harbored one or two shRNAs highly enriched relative to initial pool representation and to surrounding healthy skin; gratifyingly, this included the positive control *Brca1* shRNA (Fig. 1C). Eight candidate tumor suppressors displayed highly enriched, multiple independent shRNAs in three or more tumors (Fig. 1D). Surprisingly, *Trp53* was not among them. Subsequent analyses revealed that the *Trp53* hairpins in our pool were inefficient, and when substituted with a more potent *Trp53* shRNA, SCCs developed in our assay (fig. S6).

About 40% of tumors were enriched for four out of five shRNAs against *Myh9*, encoding non-muscle myosin IIa heavy chain (Fig. 1, C and D). Tested individually, *Myh9* shRNAs markedly reduced myosin IIa protein, and efficiency correlated strongly with tumor multiplicity (fig. S7). *Myh9* shRNA–transduced *T*β*RII*-cKO mice displayed an “open eye at

NIH-PA Author Manuscript

NIH-PA Author Manuscript

NIH-PA Author Manuscript

birth" phenotype and sparse hair coat, and although initially normal, signs of epidermal hyperproliferation appeared with age (fig. S8).

TβRII-cKO mice transduced with any of three different *Myh9* shRNAs developed multiple poorly differentiated myosin IIa–deficient skin SCCs and HNSCCs with median latencies of 3 to 7 months (Fig. 2A). Tumors displayed hallmarks of human SCCs, including invasion into subcutaneous fat, underlying muscle, and salivary glands as well as colonization to the draining lymph nodes (fig. S9). They even formed distant lung metastases (Fig. 2B). Finally, ~30% of $T\beta RII^{fl/fl}$ mice (no Cre) transduced with *Myh9* shRNAs but not scrambled shRNAs developed skin SCCs after 1 year, indicating that *Myh9* loss alone might be sufficient to promote spontaneous tumor development (Fig. 2A).

To further validate *Myh9* as an SCC tumor suppressor, we crossed $Myh9^{fl/fl}$ mice to our epithelial-specific *K14-Cre* and tamoxifen-regulated *K14CreER* deleter strains. Embryologically, *Myh9*-cKO mice recapitulated the "open eye at birth" and hair phenotypes (fig. S10, A to C). In adult mice, inducible deletion of even one *Myh9* allele concomitantly with *TβRII* ablation resulted in multiple invasive SCCs on the back, ears, and anal regions (Fig. 2C and fig. S10, C to E). Control littermates remained tumor-free during this time.

The pronounced invasion and distant metastases were linked to *Myh9* knockdown. Indeed, epithelial outgrowth from skin explants was markedly enhanced when $T\beta RII^{fl/fl}$ or *TβRII*-cKO embryos were transduced with *Myh9* but not control shRNAs (fig. S11). Similar results were obtained in vitro with scratch-wound and transwell migration as-says independent of TGF-β signaling status. Moreover, reducing *Myh9* levels profoundly affected invasion of cells through a Matrigel-coated filter (fig. S12).

These results were consistent with the well-established role for actin-myosin networks in regulating cellular movements. More puzzling was our discovery that, although *Myh9* knockdown accelerated tumor development and malignant progression upon *TβRII* ablation and under conditions favoring *HRas* mutations (fig. S13, A to E), it had very little effect on tumor latency or multiplicity in mice carrying an epithelial-specific *Trp53* gain-of-function mutation (Fig. 3A) (9). This context dependency raised the possibility that myosin IIa deficiency and *Trp53* mutations may partially overlap in function—a notion further supported by similar latencies and penetrance of spontaneous SCCs appearing in *Myh9* knockdown, *Trp53* mutant, and *Trp53* mutant–*Myh9* knockdown mice (fig. S13F). Such similarities were also observed when *Myh9* and *Trp53* knockdowns were tested on the SCC-susceptible *TβRII*-cKO background (fig. S13G).

To test for possible epistatic interactions, we treated primary keratinocytes with doxorubicin, which introduces double-strand DNA breaks, thereby triggering the DNA damage response (DDR) pathway and p53 activation (Fig. 3B) (10). Notably, expression of different *Myh9* shRNAs in keratinocytes significantly delayed and reduced p53 activation after doxorubicin treatment (Fig. 3B and fig. S14A). This was also true for $Myh9^{fl/fl}$ keratinocytes transduced in vitro with lentiviral *Cre* and for epidermis from γ-irradiated *Myh9*-cKO and *Myh9* knockdown mice (Fig. 3, C and D, and fig. S14, B to D).

NIH-PA Author Manuscript

NIH-PA Author Manuscript

NIH-PA Author Manuscript

Relative to controls, *Myh9*-deficient keratinocytes also failed to induce p53-responsive genes such as *p21, Fas, Bax, Mdm2,* and *14-3-3*σ (Fig. 3, B, D, and E). These effects were specific to the p53 pathway, because control and *Myh9* knockdown keratinocytes responded equally to other stimuli such as epidermal growth factor (EGF) (fig. S15). Moreover, such effects were not observed with shRNAs against other non-muscle myosin II genes [*Myh10* (myosin IIb) and *Myh14* (myosin IIc)], nor were they dependent on TGF-β signaling (fig. S16).

Probing deeper, we discovered that the myosin II adenosine triphosphatase (ATPase) inhibitor blebbistatin phenocopied *Myh9* loss-of-function effects on DDR-induced p53 activation (Fig. 3F and fig. S17A). Consistent with a role for myosin IIa's ATPase function, inhibition of Rho kinase, an upstream regulator of myosin II's ATPase activity, similarly dampened the DNA damage–induced p53 response. However, latrunculin-mediated inhibition of F-actin polymerization did not elicit these effects, raising the tantalizing possibility that they may be independent of myosin IIa's conventional role (Fig. 3F and fig. S17B).

The initial steps of the DDR were unperturbed, as judged by stress-induced phosphorylation of the histone variant H2AX and activation of DNA checkpoint kinases Chk1 and Chk2 (fig. S17B). Additionally, *Myh9* ablation did not affect *Trp53* transcription (Fig. 3E). However, in the presence of proteasome inhibitor MG132, p53 protein levels were comparably induced by DDR in both *Myh9* knockdown and control keratinocytes (fig. S17C).

Seeking how myosin IIa deficiency might affect p53 stability, we discovered that p53's nuclear accumulation after DNA damage did not occur upon blebbistatin treatment (Fig. 3G). Inhibiting the nuclear export receptor Crm1 restored nuclear p53 accumulation as well as transactivation of p53 target genes such as p21 (Fig. 3G and fig. S17D). Thus, when myosin IIa is defective, even though the p53 pathway can be induced in response to DNA damage, it fails to do so because of an inability of p53 to remain and/or accumulate in the nucleus.

Given the possible clinical relevance of nuclear export inhibitors as a means to overcome p53 effects in myosin IIa–defective tumors, we verified that p53 activation is similarly compromised upon myosin IIa inhibition in primary human keratinocytes (Fig. 4A). We then surveyed myosin IIa's status in >350 human skin, HNSCC, and control tissues. In contrast to normal and hyperplastic skin, which consistently displayed strong immunolabeling, 24% of skin SCCs and 31% of HNSCCs showed weak or no immunolabeling (Fig. 4B and fig. S18A). Myosin IIa was diminished in a number of early-stage (grade I) SCCs, which suggests that its loss may constitute an early event in tumor progression (fig. S18B). Additionally, when skin SCCs were analyzed according to *T*β*RII* and P-Smad2 status (6), a substantial fraction (~83%) of myosin IIa–negative tumors showed signs of concomitant loss of TGF-β signaling (fig. S18C). An initial analysis of The Cancer Genome Atlas (TCGA) showed that low *MYH9* mRNA expression significantly correlated with reduced survival of HNSCC patients (Fig. 4C), whereas patients with high *MYH9* mRNA expression or *MYH9* amplifications showed no survival changes (fig. S19, A

NIH-PA Author Manuscript

NIH-PA Author Manuscript

NIH-PA Author Manuscript

to C). As larger patient cohorts are analyzed, it will be interesting to see whether this correlation proves diagnostically relevant.

Among 302 sequenced HNSCCs, 16 non-synonymous *MYH9* mutations surfaced. Computational analyses of evolutionary conservation patterns yielded a functional impact score (FIS), which assigns a probability that a specific amino acid mutation will alter protein function (11). Intriguingly, 15 out of 16 of these *MYH9* mutations gave a high or medium FIS score (fig. S20), and when all TCGA mutations were ranked according to FIS, *MYH9* ranked 16th among the ~15,000 genes mutated in HNSCCs ($P = 0.000026$, false discovery rate $q = 0.024$) and *MYH9* was found to be mutated above background also in some other cancers (fig. S21A and tables S2 and S3).

Although this cohort of cancer-associated *MYH9* mutations is relatively small, they showed statistically significant clustering to the highly conserved ATPase switch II region (fig. S20A; $P = 0.0015$). One conserved mutation (Ala^{454}) was already known to compromise ATPase activity in *Dictyostelium* myosin II (12). Using site-directed point mutagenesis, we further corroborated the relevance of several other human mutants. Notably, although *MYH9* $Glu^{475} \rightarrow$ Lys and $Glu^{530} \rightarrow$ Lys mutants retained their ability to localize to stress fibers, they exerted dominant-negative effects on DDR-induced p53 activation (fig. S22).

Given that *Myh9* heterozygosity increased SCC susceptibility in mouse epithelia (Fig. 2C), it was also intriguing that ~15% of all HNSCCs showed hemizygous *MYH9* loss. Monoallelic *MYH9* loss was also common (~30%) in several other cancers (table S4). That said, no significant correlation existed between *MYH9* hemizygosity or *MYH9* mutations and poor HNSCC prognosis (fig. S19, D and E). Hence, although provocative, these findings await further experimental and clinical evaluation.

Finally, contrary to our expectations, *MYH9* mutations in human HNSCCs were not mutually exclusive with *Trp53* mutations (mostly gain-of-function). Although such mutual exclusiveness with oncogenic alteration of established p53 regulators (e.g., MDM2 amplifications) can exist (e.g., among glioblastomas), this paradigm does not apply to HNSCCs (fig. S23). We speculate that in HNSCCs, p53 gain-of-function mutations could confer additional effects beyond inactivation of wild-type p53, such as metastasis promotion.

Like any RNAi screen, our strategy relied on knockdown efficiency and hence invariably missed some relevant genes (e.g., *Trp53*). It also missed such genes as *Notch1*, which functions nonautonomously in SCC progression (13). These caveats aside, this methodology evaluated function within the native environment, prior to gross perturbations in tissue architecture that invariably accompany cancer progression. This unearthed some lower-penetrance genes hitherto not associated with cancer. At first glance, the inverse relation between a well-known actin-based mechano-sensitive motor and metastatic SCCs was puzzling, as dominant active Rho kinase and/or extracellular matrix stiffness can promote transformation in some cell lines and animal models (14). Although primary human cancer cells are considerably more pliable (15), and indeed our results document transforming potential, myosin IIa's most striking link to cancer appears to be in a newfound role in

NIH-PA Author Manuscript

NIH-PA Author Manuscript

NIH-PA Author Manuscript

regulating p53 stabilization and nuclear retention. These findings highlight the utility of in vivo RNAi (16) to integrate cancer genomics and mouse modeling for rapid discovery, validation, and functional characterization of potent but low-penetrance tumor suppressors.

Supplementary Material

Refer to Web version on PubMed Central for supplementary material.

Acknowledgments

We thank members of the Fuchs laboratory for helpful discussions, especially C. Luxenburg for helpful experimental suggestions and S. Dewell for deep sequencing; S. Karlsson for TβRII$^{fl/fl}$ mice; and T. Golub for sharing HNSCC data with us prior to publication. Special thanks go to the TCGA patients, the TCGA Program, and the cBIO Portal for Cancer Genomics. D.S. is an Emerald Foundation Young Investigator. D.S. was supported by the American Association for Cancer Research and the Austrian Program for Advanced Research and Technology of the Austrian Academy of Sciences. D.S. and A.S. are fellows of the Human Frontier Science Program Organization. E.F. is an Investigator of the Howard Hughes Medical Institute. Supported by NIH grant R37-AR27883 (E.F.) and Emerald Foundation Inc. The Rockefeller University has applied for a patent regarding the use of nuclear export inhibitors for the treatment of human squamous cell carcinomas, with D.S. and E.F. as inventors.

References and Notes

1. Leemans CR, Braakhuis BJ, Brakenhoff RH. Nat. Rev. Cancer. 2011; 11:9–22. [PubMed: 21160525]
2. Stransky N, et al. Science. 2011; 333:1157–1160. [PubMed: 21798893]
3. Agrawal N, et al. Science. 2011; 333:1154–1157. [PubMed: 21798897]
4. Beronja S, Livshits G, Williams S, Fuchs E. Nat. Med. 2010; 16:821–827. [PubMed: 20526348]
5. Berton TR, et al. Oncogene. 2003; 22:5415–5426. [PubMed: 12934101]
6. Guasch G, et al. Cancer Cell. 2007; 12:313–327. [PubMed: 17936557]
7. Lu SL, et al. Genes Dev. 2006; 20:1331–1342. [PubMed: 16702406]
8. Schober M, Fuchs E. Proc. Natl. Acad. Sci. U.S.A. 2011; 108:10544–10549. [PubMed: 21670270]
9. Caulin C, et al. J. Clin. Invest. 2007; 117:1893–1901. [PubMed: 17607363]
10. Schramek D, et al. Nat. Genet. 2011; 43:212–219. [PubMed: 21317887]
11. Reva B, Antipin Y, Sander C. Nucleic Acids Res. 2011; 39:e118. [PubMed: 21727090]
12. Murphy CT, Rock RS, Spudich JA. Nat. Cell Biol. 2001; 3:311–315. [PubMed: 11231583]
13. Demehri S, Turkoz A, Kopan R. Cancer Cell. 2009; 16:55–66. [PubMed: 19573812]
14. DuFort CC, Paszek MJ, Weaver VM. Nat. Rev. Mol. Cell Biol. 2011; 12:308–319. [PubMed: 21508987]
15. Fritsch A, et al. Nat. Phys. 2010; 6:730–732.
16. Beronja S, et al. Nature. 2013; 501:185–190. [PubMed: 23945586]

NIH-PA Author Manuscript
NIH-PA Author Manuscript
NIH-PA Author Manuscript

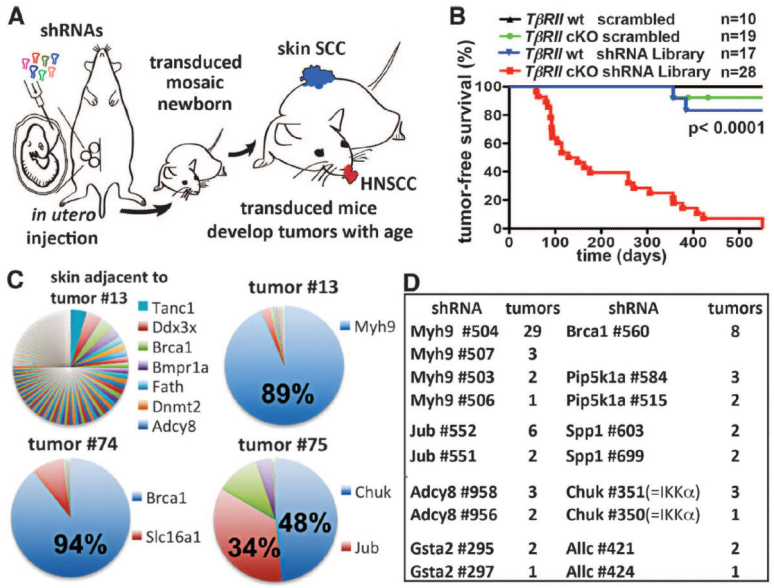

shRNA	tumors	shRNA	tumors
Myh9 #504	29	Brca1 #560	8
Myh9 #507	3		
Myh9 #503	2	Pip5k1a #584	3
Myh9 #506	1	Pip5k1a #515	2
Jub #552	6	Spp1 #603	2
Jub #551	2	Spp1 #699	2
Adcy8 #958	3	Chuk #351(=IKKα)	3
Adcy8 #956	2	Chuk #350(=IKKα)	1
Gsta2 #295	2	Allc #421	2
Gsta2 #297	1	Allc #424	1

Fig. 1. Direct in vivo shRNA screen for HNSCC tumor suppressors

(**A**) Schematic of pooled shRNA screen. (**B**) Tumor-free survival of mice of the indicated genotype transduced at E9.5 with the shRNA library targeting putative HNSCC genes (*n* = number per group; $P < 0.0001$, log-rank test). (**C**) Representative pie charts showing percent representation of a particular shRNA within an individual tumor compared to surrounding healthy skin. (**D**) Top-scoring tumor suppressor candidates and corresponding numbers of tumors showing significant enrichment.

NIH-PA Author Manuscript
NIH-PA Author Manuscript
NIH-PA Author Manuscript

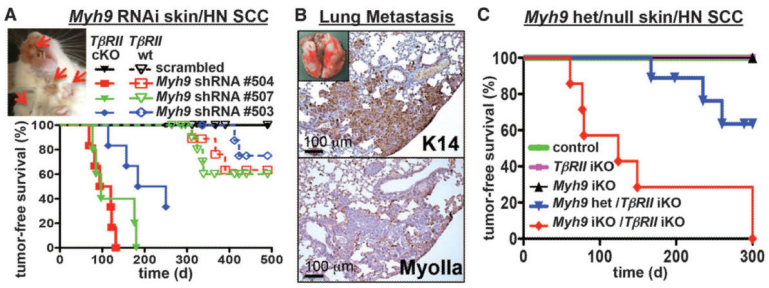

Fig. 2. Functional validation of *Myh9* as a bona fide tumor suppressor

(**A**) Tumor-free survival of mice of the indicated genotype and shRNA transduction ($n > 6$ for each genotype, $P < 0.0001$). Insert shows skin lesions (arrows) on 4-month-old *Myh9* shRNA–transduced *TβRII*-cKO mouse. (**B**) *Myh9* knockdown results in pulmonary metastases in *TβRII*-cKO mice. Metastatic lesions are immunoreactive for epithelial keratin 14 and negative for myosin IIa. (**C**) Tumor-free survival of *Myh9*/*TβRII* inducible knockout (iKO) as well as *Myh9* heterozygous/*TβRII* iKO and control mice ($n = 6$, $P < 0.001$, log-rank test).

NIH-PA Author Manuscript

NIH-PA Author Manuscript

NIH-PA Author Manuscript

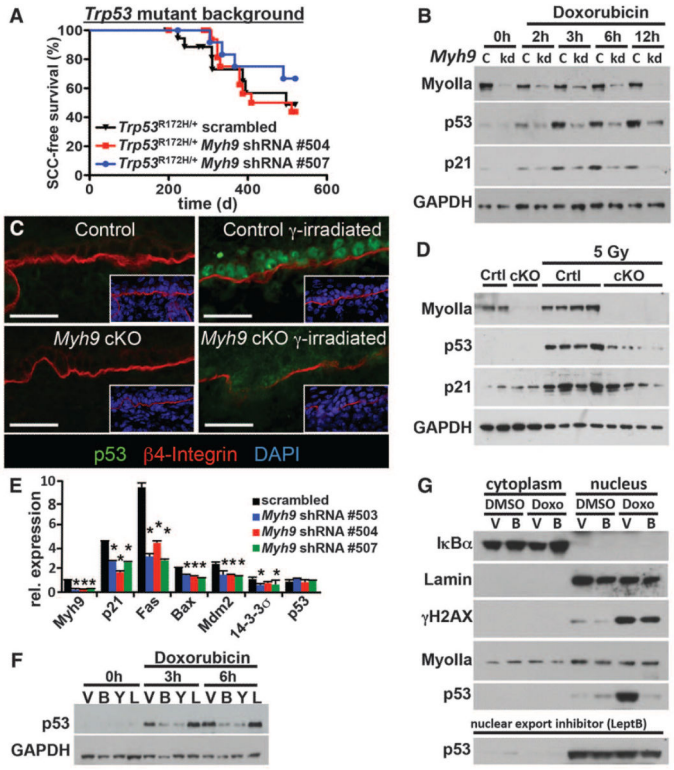

Fig. 3. A noncanonical role for myosin IIa in nuclear retention of activated p53

(**A**) Tumor-free survival of conditional *Trp53* mutant mice transduced with the indicated shRNA ($n > 6$ for each genotype; no significant survival change could be observed). (**B**) *Myh9* knockdown (kd) but not scrambled control shRNA (c) diminishes p53 and targets p21 (CDKN2) levels in response to the DDR inducer doxorubicin. Myosin IIa and GAPDH levels are shown as controls. (**C** and **D**) Lack of nuclear p53 in *Myh9*-cKO versus control (Ctrl) littermate skins 6 hours after γ irradiation (5 Gy). (C) Immunofluorescence (boxed regions show DAPI-stained nuclei in blue); (D) immunoblot analysis. Myosin IIa and GAPDH levels are shown as controls. (**E**) Quantitative polymerase chain reaction of p53 target genes illustrates the effects of *Myh9* knockdown on the p53 pathway. (**F**) p53 immunoblot of lysates from DDR-induced keratinocytes treated with vehicle (V), blebbistatin (B), Rho kinase inhibitor Y27632 (Y), or latrunculin B (L). GAPDH levels are shown as controls. (**G**) Nuclear p53 is not retained when DDR-induced *Myh9* knockdown primary keratinocytes are exposed to blebbistatin (B). Lamin A/C, IκBα, and γH2AX are controls for nuclear fraction, cytoplasmic fraction, and DDR, respectively. Nuclear export inhibitor leptomycin B rescues the ability of *Myh9*-deficient cells to retain p53 in the nucleus.

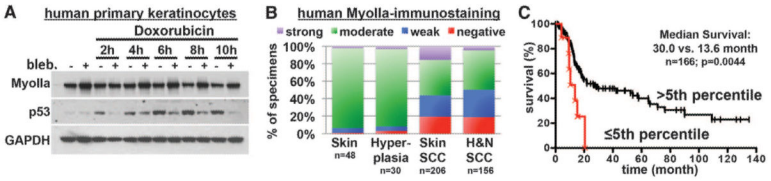

Fig. 4. *MYH9* is a bona fide tumor suppressor in human HNSCC

(**A**) p53 induction in primary human keratinocytes treated with the myosin ATPase inhibitor blebbistatin and with the DDR inducer doxorubicin. GAPDH levels are shown as loading control. (**B**) Myosin IIa quantifications on 362 samples of human healthy skin, skin SCCs, and HNSCCs. A substantial fraction of cases show absent or reduced myosin IIa expression. (**C**) Decreased *MYH9* mRNA expression correlates with shortened survival. Kaplan-Meier analysis compares overall survival of TCGA HNSCC patients stratified according to the lowest (≤5th percentile) *MYH9* expression versus the rest (>5th percentile) (n = 166, P = 0.0044, log-rank test).

NIH-PA Author Manuscript
NIH-PA Author Manuscript
NIH-PA Author Manuscript